



Alteration of magnetic mineralogy at the sulfate–methane transition: Analysis of sediments from the Argentine continental slope

J.F.L. Garming*, U. Bleil, N. Riedinger

Fachbereich Geowissenschaften, Universität Bremen, Klagenfurter, Strasse, 28359 Bremen, Germany

Received 3 September 2004; received in revised form 30 March 2005; accepted 12 April 2005

Abstract

On the Argentine continental slope off the Rio de la Plata estuary, the sulfate–methane transition (SMT) has been encountered at shallow depths of a few meters below the seafloor. At around this horizon, where sulfate diffusing downward from the bottom water is met and reduced by methane rising from deeper in the sediment column, intense alteration affects the detrital magnetic mineral assemblage. Less than 10% of the dominant primary low coercivity ferrimagnetic (titano-) magnetite remains after alteration. In the upper part of the suboxic environment, underlying the iron redox boundary, which is located at a depth of ~0.1 m, approximately 60% of the finer grained detrital fraction is already dissolved. While the high coercivity minerals are relatively unaffected in the suboxic environment, large portions (> 40%) are diagenetically dissolved in the sulfidic SMT zone. Nevertheless, the characteristics of the magnetic residue are entirely controlled by a high coercivity mineral assemblage. Unlike common observations, that diagenetic alteration produces coarser magnetic grain-sizes in suboxic milieus, a distinct overall fining is found in the sulfidic zone. Different factors should contribute to this effect. Scanning electron microscope analysis, combined with X-ray microanalysis, identified fine grained (titano-) magnetite preserved as inclusions in silicates and between high Ti titanohematite lamellae, and possibly of prime importance, a comprehensive fragmentation of larger grains in the course of maghemitization. The only secondary iron sulfide mineral detected is pyrite, which is present as clusters of euhedral crystals or directly replaces (titano-) magnetite. The thermomagnetic measurements did not provide evidence for the presence of ferrimagnetic sulfides such as greigite. Different from other studies reporting a marked magnetic enhancement at around the SMT due to the precipitation and preservation of such metastable ferrimagnetic sulfides, a complete pyritization process will cause a distinct magnetic depletion, like in the present case.

© 2005 Elsevier B.V. All rights reserved.

Keywords: Diagenesis; Sulfate reduction; Rock magnetism; Scanning electron microscope analysis

* Corresponding author. Tel.: +49 421 218 3967; fax: +49 421 218 7008.

E-mail address: garming@uni-bremen.de (J.F.L. Garming).

1. Introduction

Microbially mediated degradation of particulate organic matter drives both the iron and sulfur cycles in marine sediments (Goldhaber and Kaplan, 1974; Froelich et al., 1979). In suboxic milieus, the diagenetic dissolution of primarily ferrimagnetic (titano-) magnetite iron oxides around the iron redox boundary is a common phenomenon that has been intensively studied (e.g., Karlin and Levi, 1983; Canfield and Berner, 1987; Karlin, 1990a, 1990b; Canfield et al., 1992; Dekkers et al., 1994; Tarduno and Wilkison, 1996; Robinson et al., 2000; Passier et al., 2001; Larrasoana et al., 2003;

Reitz et al., 2004). This process affects the paleomagnetic signal with varying intensity and may jeopardize the validity of paleofield directional and intensity data (e.g., Channell and Hawthorne, 1990; Channell and Stoner, 2002).

In anoxic environments, which are typical of deeper strata, the hydrogen sulfide (H_2S) needed for the formation of (iron) sulfides is produced by the biogenic reduction of sulfate (SO_4^{2-}), either by degradation of organic matter or by oxidation of methane (CH_4). Boetius et al. (2000) found that in sediments containing gas hydrates, sulfate reducing bacteria form aggregates with archaea that oxidize methane. The coupled

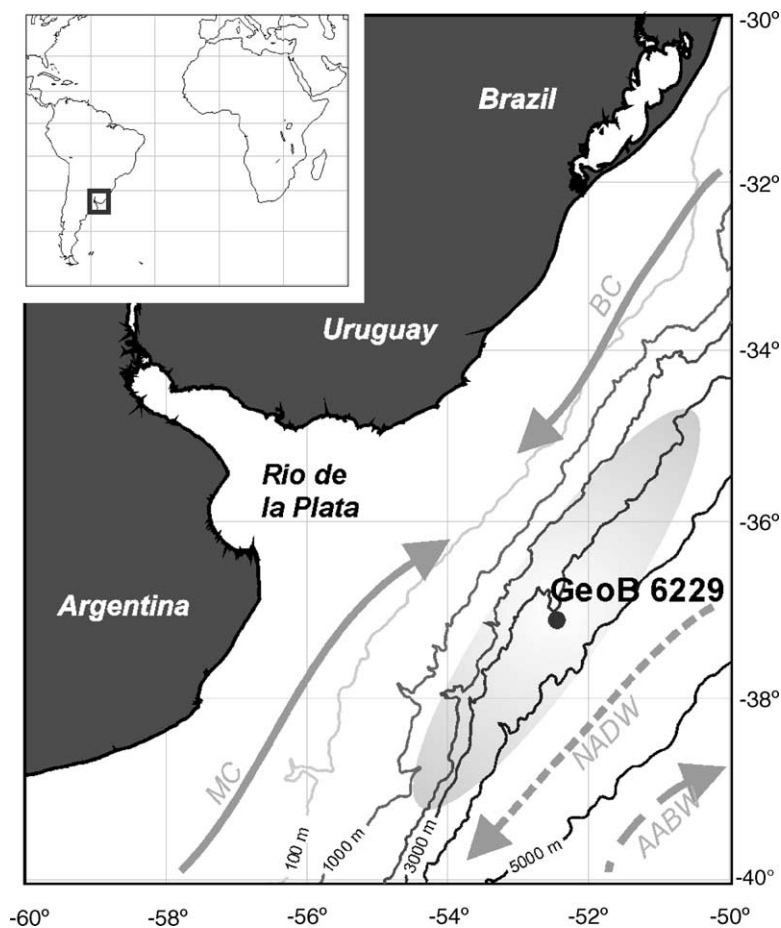


Fig. 1. Map of the South American continental margin off the Rio de la Plata estuary. Arrows indicate simplified main flow paths of surface (MC, Malvinas Current; BC, Brazil Current), deep (NADW, North Atlantic Deep Water) and bottom (AABW, Antarctic Bottom Water) water masses. Shading around the core site GeoB 6229 outlines the area where distinct ‘susceptibility gaps’ were found in the sedimentary deposits (see text). Isobaths at 1000 m intervals, including the 100 m isobath, are according to GEBCO (redrawn after Frenz et al., 2004).

sulfate–methane reaction is proposed to proceed according to the following equation assuming a one-to-one stoichiometry (Niewöhner et al., 1998):



The depth of this sulfate–methane reaction, called the sulfate–methane transition (SMT), depends on the penetration depth of seawater sulfate into the sediments and on the intensity of the methane flux from deeper sediment layers. Borowski et al. (1996) proposed that sulfate pore water profiles with constant gradients above the transition zone are indicative of anaerobic oxidation of methane (AOM) controlling the sulfate reduction.

Numerous pore water profiles from the Argentine continental slope show approximately linear sulfate gradients to unusually shallow penetration depths of about 4–6 m (Bleil et al., 1994; Schulz et al., 2001; Hensen et al., 2003; Riedinger et al., *in press*). At around the SMT, magnetic susceptibility, which is routinely measured directly after core recovery on board the research vessel, exhibits pronounced minima. Susceptibility is characteristically reduced by 80% or more over depth intervals of several meters relative to the sedimentary layers above and below, indicating large-scale alteration of the magnetic mineral assemblage. In Fig. 1, the shaded area in front of the Rio de la Plata estuary, ranging from about 1500 to 4000 m water depth, outlines the region where such ‘susceptibility gaps’ have been observed (Bleil et al., 1994, 2001; Schulz et al., 2001). They are thought to ultimately result from a depth fixation of the SMT for a prolonged period of time, with intense magnetic iron oxide dissolution occurring at around the SMT (Riedinger et al., *in press*). A marked change from high sedimentation rates during the last glacial period to low Holocene accumulation has been proposed to be the cause of a rapid rise of the SMT from deeper positions and its stagnation at the present horizon, after which steady state conditions for the sulfate–methane reaction were established (Kasten et al., 1998; Riedinger et al., *in press*).

Sparse information is currently available about diagenetic alteration of magnetic oxides/hydroxides and the potential formation of magnetic iron sulfide minerals in SMT environments. This topic will be discussed here on the basis of comprehensive rock magnetic analyses and scanning electron microscope (SEM) analy-

sis combined with X-ray microanalyses for sediments from the Argentine continental slope.

2. Study area

The highly dynamic sedimentation processes along the Argentine continental margin are controlled by strong surface and bottom water currents as well as gravity driven mass flows. The fluvial load discharged by a number of large and small rivers is generally not deposited near the coast, but is transported to deeper water by offshore currents and turbidites (Ewing et al., 1964). Post-glacial sedimentation rates of around 25–50 cm/kyr on the shelf and continental slope (Haese, 1997) and 0.5–5 cm/kyr in the western abyssal plain region (Stevenson and Cheng, 1969; Ewing et al., 1971) have been reported. Fine grained sediment components are known to be transported far into the central basin by bottom currents, which produce massive nepheloid layers, drift deposits and mudwaves (Ewing et al., 1971; Ledbetter and Klaus, 1987; Manley and Flood, 1993; Richardson et al., 1993).

Modern oceanographic studies differentiate more than eight individual water masses along the western boundary of the South Atlantic (e.g., Memery et al., 2000; Frenz et al., 2004). Sub-Antarctic waters (SAW) and subtropical waters (STW) are present in the upper 500 m of the water column. Combined with Antarctic Intermediate Water (AAIW), which flows in the depth interval from about 500 to 1500 m, SAW forms the Malvinas (Falkland) Current (MC), and STW forms the Brazilian Current (BC). In the area of the Rio de la Plata estuary, these currents merge in the Malvinas-Brazil Confluence (MBC) and are deflected to the southeast. In the depth range from 2000 to 4000 m, North Atlantic Deep Water (NADW) flows southward as far as 45°S. Below, northward directed Antarctic Bottom Water (AABW) forms a strong contour current (Fig. 1).

The sediments investigated were recovered in a gravity core at station GeoB 6229 (37°12.4'S/52°39.0'W) during R/V Meteor Cruise M46/2 (Schulz et al., 2001) from a water depth of 3446 m in front of the Rio de la Plata estuary (Fig. 1). The suspended load of its two major tributaries, the Uruguay and Paraná rivers, is dominated by clays. These loads are carried away to the north, forming a sedimentary tongue parallel to the coast of Uruguay (Ewing et al., 1964; Frenz

et al., 2004), whilst the coarser fraction is transported directly down slope. Relatively coarse grained sediments were therefore retrieved at station GeoB 6229, which predominately consist of lithogenic components. XRD analyses (Riedinger et al., in press) indicate that some 90% of the deposits are composed of quartz, feldspar and phyllosilicates. Considering the drainage areas of the Uruguay and Paraná rivers, the detrital magnetic mineral component of the sediment should primarily originate from the Paraná volcanic province. While calcium carbonate concentration is low (< 5 wt%), relatively high amounts of organic carbon, about 1.1 wt% in the top layers and overall on average 0.7 wt%, provide evidence for elevated regional marine biologic productivity.

3. Laboratory procedures

3.1. Sampling

Sediments from the 9.27 m core GeoB 6229 mostly consist of uniform olive green-gray mud with increasing numbers of black spots at greater depths. Upon recovery, the sediments smelled strongly of H₂S.

For shipboard pore water analysis and subsequent shore-based geochemical and rock magnetic investigations, the sediments were sampled at 10–20 cm intervals. A supplementary series of cube specimens (6.2 cm³) was taken exclusively for rock magnetic purposes.

3.2. Geochemical and rock magnetic analyses

Shipboard pore water measurements comprised quantification of SO₄²⁻, CH₄, H₂S and Fe²⁺. Solid phase analyses and sequential iron extraction were subsequently performed in the University of Bremen laboratories. An overview of the experimental methods is available at <http://www.geochemie.uni-bremen.de/links.html> (for more detailed information see: Schulz et al., 1994; Haese et al., 1997; Niewöhner et al., 1998; Hensen et al., 2003; Riedinger et al., in press).

Hysteresis and thermomagnetic cycling experiments, as well as magnetic mineral separation extracts, were made on freeze-dried splits of the geochemical samples. Miniature specimens for hysteresis measurements were prepared with a technique described by von

Dobeneck (1996), while the routine of Petersen et al. (1986) was applied for magnetic mineral extraction.

Magnetic hysteresis measurements limited to a maximum field of 0.3 T were performed with a PMCM2900 alternating-gradient force magnetometer. For data processing, the program 'Hystear' (von Dobeneck, 1996) was used to determine mass specific saturation magnetization σ_s and remanent saturation magnetization σ_{rs} , coercive force B_c and remanent coercivity B_{cr} , all of which specify characteristics of the ferrimagnetic (titano-) magnetite mineral components. Additionally, the non-ferromagnetic susceptibility χ_{nf} , which quantifies paramagnetic and diamagnetic contributions of the sedimentary matrix to susceptibility, has been inferred from these measurements with an approach-to-saturation analysis (von Dobeneck, 1996).

For 10 selected samples, thermomagnetic runs to maximum temperatures of 720 °C were performed with a modified horizontal translation type Curie balance (Mullender et al., 1993) on 20–30 mg of bulk sediment weighed into a quartz glass sample holder open to air and held in place by quartz wool. Heating rates were 10 °C/min, while cooling rates were 15 °C/min.

Magnetic extracts of the same 10 selected samples were molded into epoxy resin for SEM analysis. Thin sections were examined and photographed with a XL30 SFEQ instrument. X-ray microanalysis was performed with an energy dispersive spectroscopy (EDS) detector unit.

Magnetic susceptibility per volume κ was determined at 1 cm spacing on the split sediment surface of core GeoB 6229 archive halves using a Bartington Instruments MS2 F sensor. Bulk rock magnetic measurements were accomplished on cube specimens taken at an average of 5 cm depth intervals. Incremental acquisition of isothermal remanent magnetization (M_{IR}) to 0.3 T and incremental acquisition of anhysteretic remanent magnetization (M_{AR}), imparted by superimposing a gradually decaying alternating field (AF) of 0.3 T maximum amplitude to a constant bias field of 40 μ T was followed by systematic (18 steps) AF demagnetization to a maximum field of 0.3 T. All remanences were measured on a 2G Enterprises 755R DC SQUID cryogenic magnetometer system. The various applied fields were generated with its built-in facilities. A number of specific rock magnetic parameters that characterize the ferrimagnetic (titano-) magnetite mineral fraction were deduced from these data sets,

including the median acquisition field, $B_{1/2} M_{\text{IRA}}$, and the median destructive fields $B_{1/2} M_{\text{AR}}$ and $B_{1/2} M_{\text{IR}}$.

To estimate high coercivity hematite/goethite concentrations from the hard isothermal remanent magnetization M_{HIR} (Stoner et al., 1996), detailed M_{IR} acquisition was continued to 2.5 T, the maximum field available for an external 2G Enterprises 660 pulse magnetizer. At this stage, a 0.3 T backfield was applied. M_{IR} acquisition data were also used to perform a component analysis with a modified version of the *Irmunmix 2.2* program developed by Heslop et al. (2002). Plotted against the logarithm of the acquisition field, incremental M_{IR} results in a simple sigmoid shaped curve, which is essentially a cumulative log Gaussian curve (or a combination of such curves) representing the coercivity distribution of the constituent magnetic minerals (Robertson and France, 1994; Kruiver et al., 2001). The *Irmunmix* software utilizes an expectation maximization algorithm to automatically separate M_{IR} contributions of (typically two or three) individual components.

4. Results

4.1. Geochemistry

Pore water analyses have identified the SMT at a depth of approximately 5.5 m (Riedinger et al., in press). The virtually linear decrease of sulfate from the top layers to this level (Fig. 2) indicates a dynamic equilibrium between downward sulfate diffusion and the methane flux rising from deeper sources (Borowski et al., 1996; Niewöhner et al., 1998; Hensen et al., 2003). Around the SMT, free sulfide generated by AOM is observed in the pore water. Gas hydrates were not encountered in the sediment sequence, but are likely to exist in deeper strata of the Argentine continental margin (Gornitz and Fung, 1994).

The presence of sulfide in the pore waters gave reason for subdividing the sediment sequence into three sections, (1) an upper part, from the top to 3.9 m, (2) a sulfidic zone ranging from 3.9 to 6.6 m and (3) a lower part, from 6.6 m to the bottom of the core at 9.27 m depth. In the upper part of the core and in the sulfidic zone, little to no iron (Fe^{2+}) was detected in the pore waters, whereas this redox sensitive element is present in the pore waters of the lower part of the core (Fig. 2). Solid phase analyses (shown in Riedinger

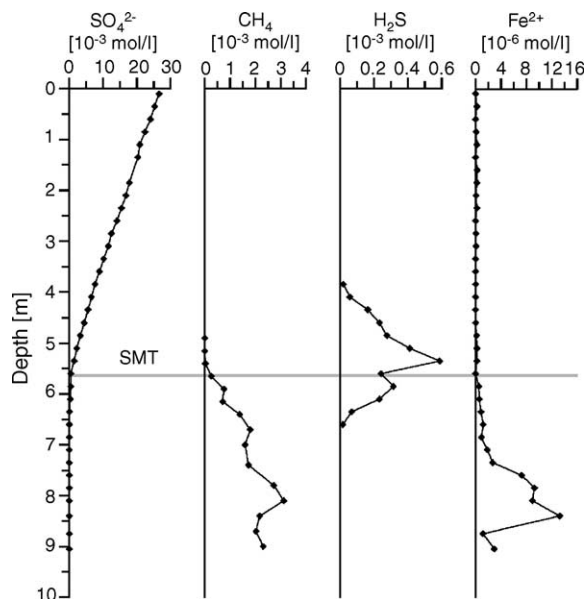


Fig. 2. Sulfate, methane, sulfide, and iron pore water profiles as measured directly after recovery of the sediments. The horizontal line indicates the approximate position of the sulfate–methane transition (SMT). Data are taken from Riedinger et al. (in press).

et al., in press) did not reveal an enhanced accumulation of Fe^{2+} in the sediments of the sulfidic zone, but they did indicate slightly elevated sulfur contents.

4.2. Magnetic mineral inventory

4.2.1. Mineralogy and concentration

Variations in (titano-) magnetite content, delineated by the hysteresis parameters σ_s and σ_{rs} as well as M_{AR} and M_{IR} (all referring to peak fields of 0.3 T), are illustrated in Fig. 3, together with κ . Respective arithmetic means for the upper part, the sulfidic zone and the lower part of the sediment sequence are listed in Table 1. Note that the intervals from 3.5 to 4.2 m between the upper part and the sulfidic zone and from 6.1 to 7.1 m between the sulfidic zone and the lower part, where all magnetic properties exhibit strong gradients, have been excluded from these calculations.

Saturation magnetization σ_s , which is the only strictly grain-size independent measure of magnetic mineral concentration, displays a distinct decrease in the sulfidic zone to $9.4 \times 10^{-3} \text{ A m}^2/\text{kg}$ compared to 118.5×10^{-3} and $110.4 \times 10^{-3} \text{ A m}^2/\text{kg}$ in the upper

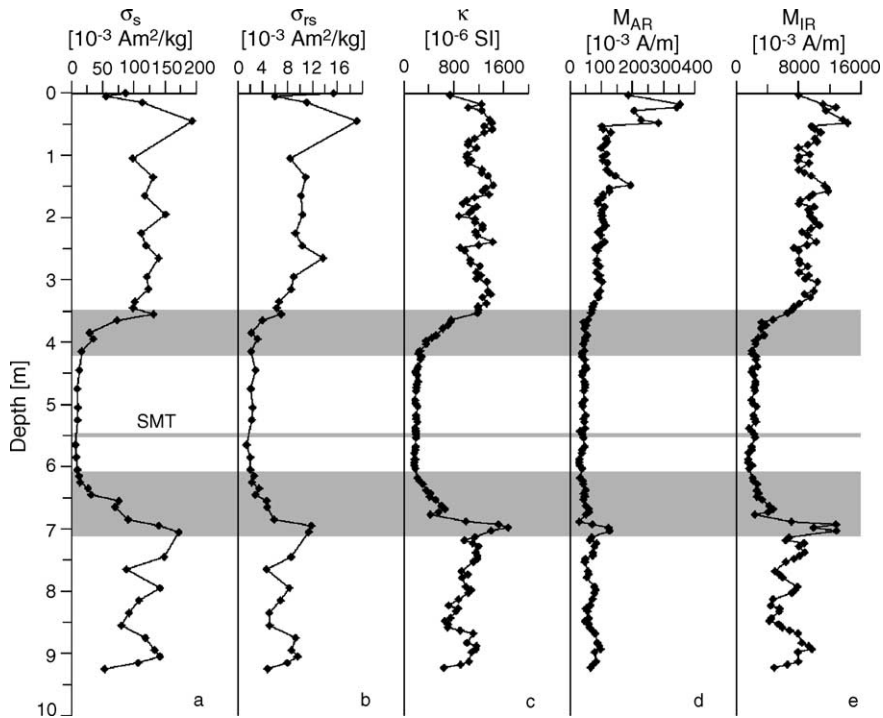


Fig. 3. Depth profiles of rock magnetic parameters that delineate variations in magnetic mineral content. Mass specific (a) saturation magnetization σ_s , and (b) remanent saturation magnetization σ_{rs} , volume specific (c) low field magnetic susceptibility κ , (d) anhysteretic remanent magnetization M_{AR} , and (e) isothermal remanent magnetization M_{IR} . Gray shaded areas mark the transitions between the sulfidic zone and the upper and lower sediment series. The horizontal line indicates the approximate position of the sulfate–methane transition (SMT).

and lower sediments, respectively (Fig. 3a). This more than 90% decrease is clearly indicative of reductive dissolution of the ferrimagnetic mineral fraction and corresponds to a similar, somewhat less pronounced decline in saturation remanence, σ_{rs} (Fig. 3b). It is also consistent with the susceptibility profile (Fig. 3c). Differences in these concentration related parameters between the sediments above and below the sulfidic zone are minor for σ_s (–7%), but are significant for σ_{rs} (–29%) and κ (–17%). This likely hints at grain-size effects, namely the presence of higher amounts of fine to very fine grained (titano-) magnetite in the upper part of the core.

Single-domain (SD) and small pseudo-single-domain (PSD) crystals acquire the strongest anhysteretic remanent magnetizations (Banerjee et al., 1981). The decrease in M_{AR} intensity in the sulfidic zone, from on average 121×10^{-3} A/m in the upper part, to 42×10^{-3} A/m (Fig. 3d), is noticeably less pronounced than for M_{IR} , which quantifies the total ferrimag-

netic mineral component (9476 to 2146×10^{-3} A/m, Fig. 3e). In view of previous evidence, that fine grained magnetite undergoes diagenetic dissolution more rapidly than coarse grained magnetite due to its larger surface area to volume ratio, this apparent grain-size fining appears to be puzzling. As indicated by the sharp intensity decline in the M_{AR} profile (Fig. 3d), from a mean of 267×10^{-3} A/m in the uppermost 0.5 m to 104×10^{-3} A/m below, the principal reductive dissolution of the fine grained ferrimagnetic fraction appears to have already occurred in the top most part of the sediment column. It is associated with the modern iron redox boundary, which is located at ~ 0.1 m, although no characteristic change in color (Lyle, 1983) or conspicuous features in the pore water data (Fig. 2) were observed at around this level. In the suboxic environment, only 39% of the original fine grained ferrimagnetic fraction is left, as inferred from M_{AR} , compared to 77% of the coarser grained portion, as inferred from M_{IR} . In the sulfidic zone, 16% of the M_{AR} and 18%

Table 1

Average rock magnetic parameters for the upper part, the sulfidic zone and the lower part of the studied sediment sequence

Parameter	Upper part	Sulfidic zone	Lower part
σ_s (10^{-3} A m ² /kg)	118.5	9.4	110.4
σ_{rs} (10^{-3} Am ² /kg)	10.1	2.2	7.2
κ (10^{-6} SI)	1179	200	974
M_{AR} (10^{-3} A/m)	121.4	41.9	69.3
M_{IR} (10^{-3} A/m)	9476	2146	6751
M_{HIR} (10^{-3} A/m)	425	240	340
S-ratio	0.98	0.95	0.98
χ_{nf}/χ	0.03	0.40	0.05
B_c (mT)	8.2	18.3	6.6
B_{cr} (mT)	31.7	62.2	32.4
$B_{1/2} M_{AR}$ (mT)	30.2	57.0	37.1
$B_{1/2} M_{IR}$ (mT)	17.1	49.9	17.2
C1 $B_{1/2} M_{IRA}$ (mT)	39.0	42.2	37.2
C2 $B_{1/2} M_{IRA}$ (mT)	81.9	90.5	69.9
C3 $B_{1/2} M_{IRA}$ (mT)	1000	887	416
C1 % M_{IR}	57.9	11.7	54.0
C2 % M_{IR}	39.8	75.6	40.7
C3 % M_{IR}	2.3	12.7	5.3
σ_{rs}/σ_s	0.09	0.23	0.07
B_{cr}/B_c	3.98	3.45	4.90
M_{AR}/M_{IR}	0.01	0.02	0.01
κ_{AR}/κ	3.3	6.6	2.3

of the M_{IR} intensities remain. The persisting (titano-) magnetite minerals are presumably protected against diagenetic dissolution (e.g., as inclusions in a silicate matrix). Below the sulfidic zone, M_{AR} and M_{IR} increase to 69×10^{-3} and 6751×10^{-3} A/m, respectively, corresponding to 26 and 56% of the intensities in the top layer of the core. This implies that diagenetic alteration has also affected the lower section of the core, possibly when the SMT rapidly ascended to its present horizon from a deeper position (Riedinger et al., in press) and from that time on, while it was in an anoxic methanic environment.

To evaluate variations in other magnetically relevant minerals, the hard isothermal remanent magnetization M_{HIR} , the S-ratio and the χ_{nf}/χ ratio were examined (Fig. 4, Table 1). M_{HIR} (Stoner et al., 1996) quantifies contributions of high coercivity iron oxides (hematite, hemoilmenite) and iron hydroxides (e.g., goethite) to the total remanence. In the upper part of the core, it amounts to on average 425×10^{-3} A/m (Fig. 4a). Assuming a hematite to (titano-) magnetite saturation

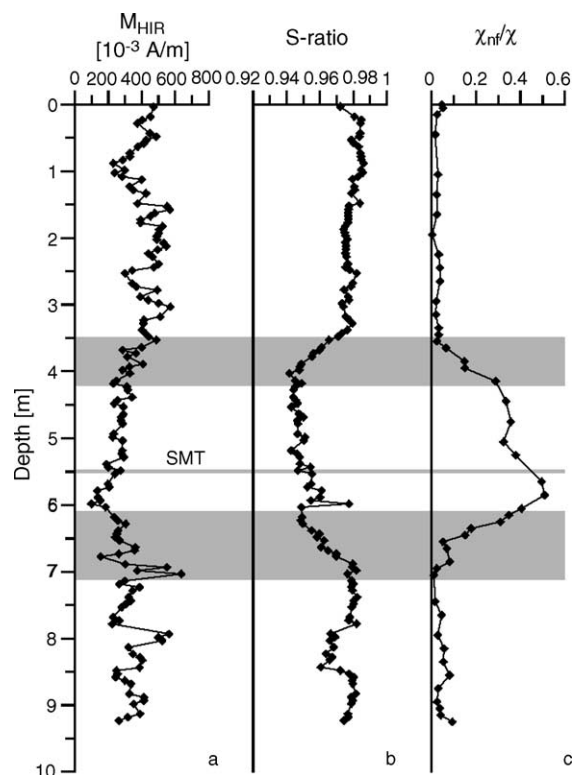


Fig. 4. Depth profiles of rock magnetic parameters that characterize variations in magnetic mineralogy. (a) Hard isothermal remanent magnetization M_{HIR} quantifies contributions of high coercivity iron oxides and hydroxides to the total remanence (Stoner et al., 1996), (b) the S-ratio provides an estimate of the relative proportions of hard and soft magnetic minerals (Bloemendal et al., 1992), (c) the χ_{nf}/χ ratio estimates paramagnetic sediment matrix contributions to the bulk magnetic susceptibility. Gray shaded areas mark the transitions between the sulfidic zone and the upper and lower sediment series. The horizontal line indicates the approximate position of the sulfate–methane transition (SMT).

remanence proportion of 1:10, implies that hematite makes up approximately one third of the total magnetic mineral assemblage. This admittedly rough estimate nevertheless suggests a much lower hematite content than is generally observed in the South Atlantic, particularly in areas with significant deposition of eolian terrigenous material. In the sulfidic zone, M_{HIR} drops by 44% to 240×10^{-3} A/m, which indicates that high coercivity minerals are also diagenetically dissolved in this environment, although they are relatively more stable than the ferrimagnetic oxides, as was recently also shown by Yamazaki et al. (2003), Liu et al. (2004) and

Emiroglu et al. (2004). Compared to the upper part of the core, the 20% lower M_{HIR} in the sediments under the sulfidic zone suggests some minor diagenetic alteration. S -ratios calculated after Bloemendal et al. (1992) are on average 0.98 in the upper and lower sediment series (Fig. 4b) and confirm comparatively minor primary high coercivity mineral concentrations. Because of the drastically diminishing ferrimagnetic fraction in the sulfidic zone, the S -ratio drops to 0.95 and the relative content of high coercivity minerals increases to somewhat more than 50%.

The χ_{nf}/χ ratio (Fig. 4c), which provides an estimate of the contribution of non-ferromagnetic sediment matrix constituents to bulk susceptibility, is successfully used to separate distinctly different depositional regimes or to delimit zones of diagenetic alteration (Frederichs et al., 1999). Continually low ratios of 0.03 and 0.05 are observed in the upper and lower parts of the core. In the sulfidic zone, substantially more iron is bound in paramagnetic compounds, the χ_{nf}/χ ratio increases to an average of 0.4 and reaches maxima of up to 0.5. This essentially records the combined effects of ferrimagnetic and also of high coercivity mineral dissolution by reductive diagenesis and a concurrent precipitation of Fe-bearing paramagnetic minerals. As indicated by slightly enhanced sulfur concentrations in the solid phase (Riedinger et al., *in press*), the formation of pyrite should be of particular importance in this respect.

4.2.2. Coercivity and IRM component analysis

Depth profiles of coercivity parameters B_c and B_{cr} derived from hysteresis measurements to maximum fields of 0.3 T and medium destructive fields $B_{1/2}$ of M_{AR} and M_{IR} (both acquired in 0.3 T fields) reveal remarkably different patterns compared to the concentration indicative parameters (Fig. 5, Table 1). Coercivities are relatively low and show limited variability within the upper and lower parts of the sediment column. Strikingly higher coercivities in the sulfidic zone result in an approximately twofold increase of B_c , B_{cr} and $B_{1/2} M_{\text{AR}}$ and even an almost threefold increase of $B_{1/2} M_{\text{IR}}$.

All of these parameters can be used as sensitive indicators of grain-size provided that the mineralogy is reasonably uniform (Thompson and Oldfield, 1986). In this scenario, multi-domain (MD) grains have substantially lower coercivities than PSD or SD grains. Under

the assumption of uniform mineralogy, the observed strong increase in coercivity in the sulfidic zone would imply a change to predominantly finer grained magnetic mineral assemblage, a conclusion that is not in agreement with the above discussed variations in M_{AR} and M_{IR} .

To achieve more insight into this problem, an IRM component analysis has been performed to discriminate between magnetization components. The three component solution is illustrated in Fig. 6 and is summarized in Table 1. It results in a ‘soft’ component (C1), with an average half IRM acquisition field $B_{1/2} M_{\text{IRA}}$ of around 40 mT, in all three parts of the sediment column and should exclusively incorporate the (titano-) magnetite fraction. In the upper and lower sediment sections, where these minerals largely dominate the magnetic inventory, $B_{1/2} M_{\text{IRA}}$ of C1 plausibly corresponds to the bulk B_{cr} data. Considerably higher coercivities characterize the second component C2 for which average $B_{1/2} M_{\text{IRA}}$ of 82.0, 90.5 and 69.9 mT were determined in the upper part, the sulfidic zone and the lower part, respectively. Apparently, there is no straightforward interpretation of this ‘hard’ component in terms of an individual mineral fraction. Hematite of appropriate grain-size (Kletetschka and Wasilewski, 2002), but also titanomagnetites with higher titanium contents and/or elevated oxidation states could be the carrier of C2 which is therefore tentatively termed a hard (titano-) magnetite/hematite component. The second high coercivity constituent, labeled goethite/hematite component C3, since it should mainly reside in goethite possibly with some hematite contributions, displays a continuous trend of declining $B_{1/2} M_{\text{IRA}}$ with depth, averaging 1000, 887 and 416 mT in the upper part, the sulfidic zone and the lower part, respectively.

Relative contributions of the three components to the total isothermal remanent magnetization contrast in the different sediment sections. The soft (titano-) magnetite component C1 dominates in the upper and lower part and comprises 58 and 54%, respectively. In the sulfidic zone, it is reduced to on average only 12%. The opposite trend is found for the hard (titano-) magnetite/hematite component C2, which contributes about 40% in the upper and lower part of the core and 76% in the sulfidic zone. The high coercivity goethite/hematite component C3 is of minor importance, carrying only 2 and 5% of the total remanence in the upper and

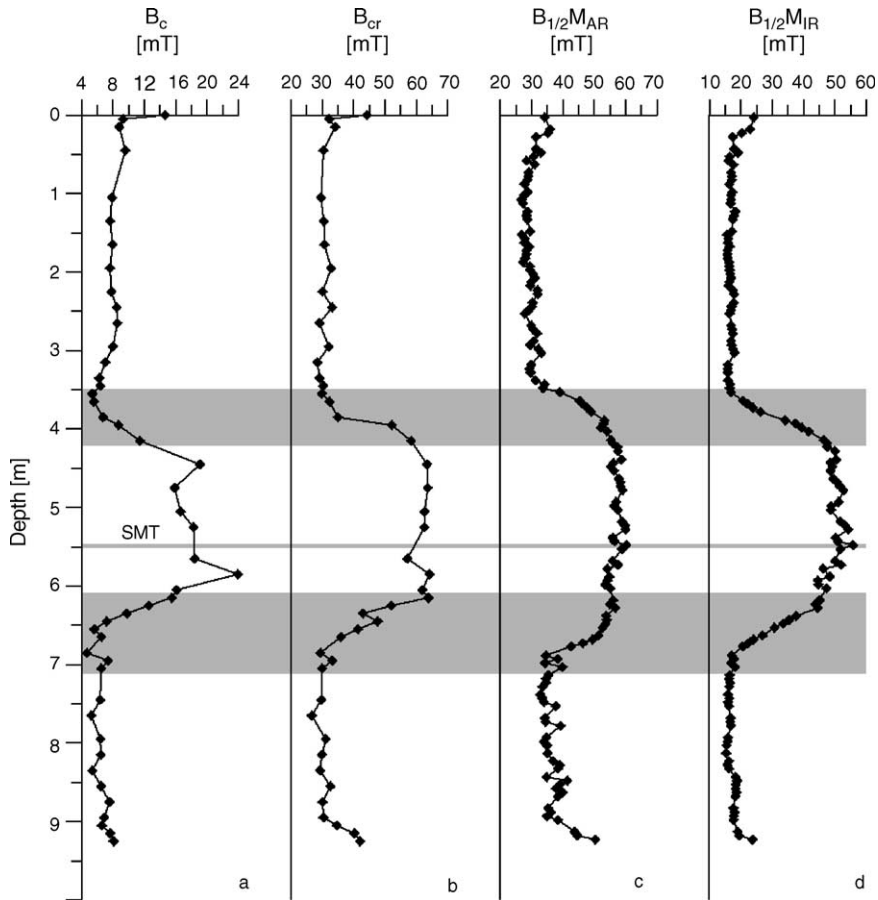


Fig. 5. Depth profiles of rock magnetic parameters that characterize variations in magnetic coercivity. (a) Coercive field B_c , (b) remanent coercive field B_{cr} , (c) median destructive field of the anhysteretic remanent magnetization $B_{1/2} M_{AR}$, and (d) median destructive field of the isothermal remanent magnetization $B_{1/2} M_{IR}$. Gray shaded areas mark the transitions between the sulfidic zone and the upper and lower sediment series. The horizontal line indicates the approximate position of the sulfate–methane transition (SMT).

lower part of the core. It rises to on average 13% in the sulfidic zone, where it is highly variable. Compared to components C1 and C2, which should be reliably defined, several limitations may affect C3. Most important is the restriction to 2.5 T maximum fields, which is far too low to saturate goethite and hence to appropriately evaluate such a mineral fraction with the *Irmunmix* program. It should therefore not be regarded as a quantitative measure, but as an indication that such a high coercivity component is present in the sediments.

The IRM component analysis provides convincing evidence for a marked shift in coercivity associated

with a change in predominant magnetic mineralogy between the upper and lower sediment series and the sulfidic zone. Preferential dissolution of the soft (titano-) magnetite component in the sulfidic zone leaves the hard (titano-) magnetite/hematite component as the principal carrier of remanence. Apparently, it also largely controls M_{AR} , M_{IR} and the hysteresis data (measured in maximum fields of 0.3 T).

4.2.3. Grain-size

The hysteresis parameter ratios σ_{rs}/σ_s (Fig. 7a) and B_{cr}/B_c (Fig. 7b) are popular measures to characterize the bulk (titano-) magnetite grain-size distribution (Day

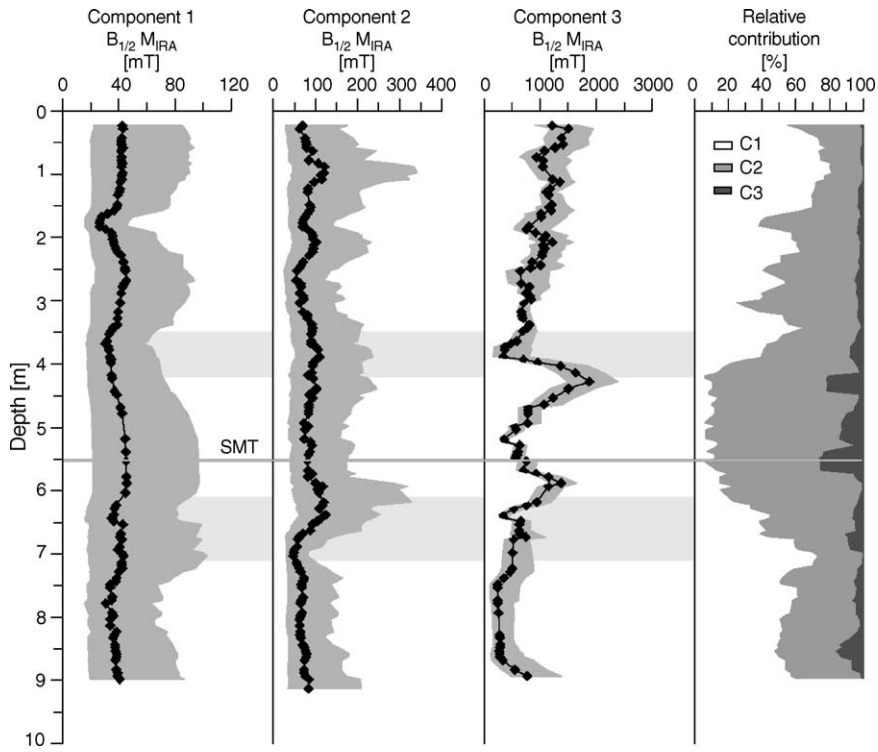


Fig. 6. Results of IRM component analysis. Black diamonds represent the 5-point mean, shading the standard deviation of coercivities obtained for a 3-component solution that discriminates a ‘soft’ (titano-) magnetite component, a ‘hard’ (titano-) magnetite/hematite component and a ‘highest coercivity’ goethite/hematite fraction. Variations in the relative contribution of individual components to the isothermal remanent magnetization are shown in the right-hand panel. Gray shaded areas mark the transitions between the sulfidic zone and the upper and lower sediment series. The horizontal line indicates the approximate position of the sulfate–methane transition (SMT).

et al., 1977; Dunlop, 2002). They indicate relatively coarse grain-sizes spectra above and below the sulfidic zone, where these minerals dominate. More MD-like data in the lower part probably documents a relatively mild alteration that mainly affected the finer grained ferrimagnetic oxides. In the sulfidic zone, a mean of 0.23 for σ_{rs}/σ_s and 3.5 for B_{cr}/B_c (lowest B_{cr}/B_c are around 2.7) approach the medium PSD range suggesting an apparent grain-size fining.

The M_{AR}/M_{IR} and κ_{AR}/κ ratios (Fig. 7c and d), also widely used magnetic grain-size indicators (Maher, 1988; Heider et al., 1996), show slightly elevated concentrations of fine grained (titano-) magnetite in the uppermost layers. As already seen in the M_{AR} data, fine grained (titano-) magnetite disappears at a depth of 0.5 m, being dissolved in the suboxic environment below the iron redox boundary. M_{AR}/M_{IR} ratios and κ_{AR}/κ ratios confirm the coarse grained magnetic min-

eral inventory recognized in the hysteresis data. The same is true for the relatively finer grain-size spectra in the sulfidic zone, which is indicated by increasing M_{AR}/M_{IR} and κ_{AR}/κ ratios.

The shift to smaller magnetic grain-sizes in an environment of strong diagenetic alteration is an unexpected result. Numerous reports in the literature and our own experience typically indicate the opposite trend. However, considering an initially coarse grained iron oxide mineral assemblage, dissolution will inevitably result in overall finer grain-sizes. This process has necessarily affected the hard (titano-) magnetite/hematite component, which is by far the dominant magnetic mineral fraction in the sulfidic zone. Increasing coercivities in these sediments should therefore to some extent result from decreasing magnetic grain-sizes.

On the other hand, the possible diagenetic formation of magnetic iron sulfides, like greigite, could

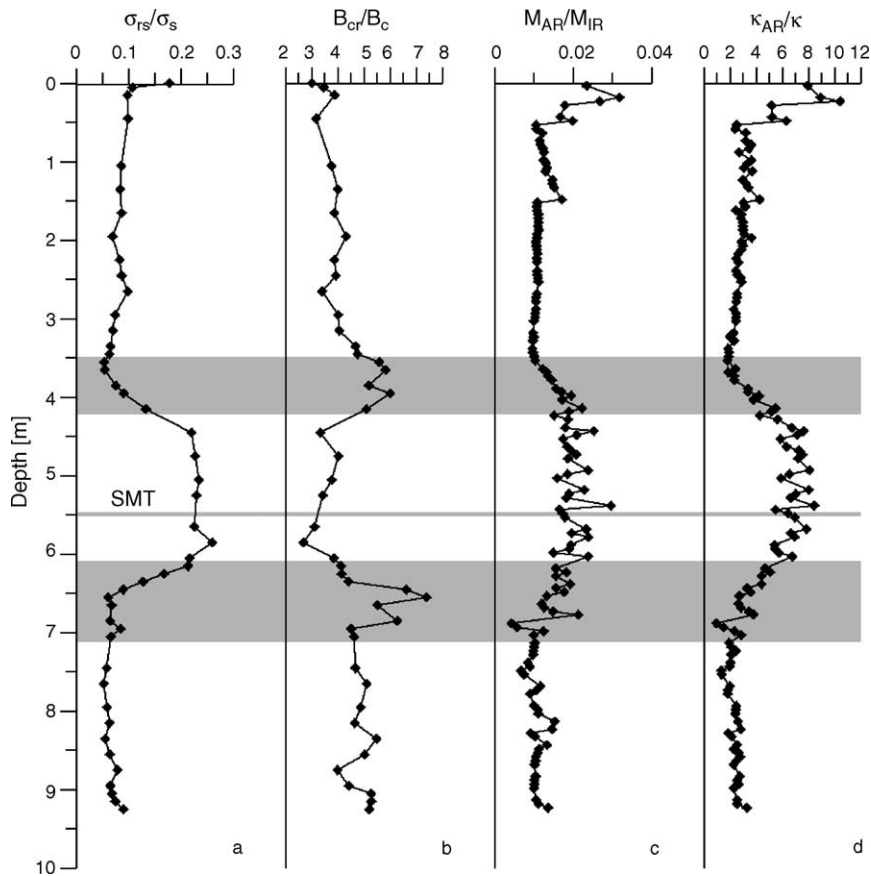


Fig. 7. Depth profiles of rock magnetic parameters that characterize magnetic grain-size variations. Bulk magnetogranulometric ratios of (a) saturation magnetization to saturation remanence σ_{rs}/σ_s , and (b) coercivity of remanence to coercive field B_{cr}/B_c , (c) M_{AR}/M_{IR} , and (d) κ_{AR}/κ ratios, which delineate variations in the fine grained magnetic fractions. Gray shaded areas mark the transitions between the sulfidic zone and the upper and lower sediment series. The horizontal line indicates the approximate position of the sulfate–methane transition (SMT).

also be responsible for a fining of the magnetic grain-sizes (Roberts et al., 1999; Liu et al., 2004). In a recent study Neretin et al. (2004) identified two processes of diffusion limited pyrite formation surrounding the SMT. One involved the precipitation of pyrite precursors including ferrimagnetic greigite.

4.2.4. Thermomagnetic analyses

Significant Curie temperatures in the upper and lower part of the sediment sequence are around 580 °C (Fig. 8), which identifies magnetite as the predominant magnetic phase. Minor inflections between 300 and 500 °C in the heating records hint at titanomagnetite with variable titanium content. The continu-

ous decrease of magnetization upon heating may imply a broad range of titanomagnetite compositions. At 720 °C, the magnetic Fe oxides are largely destroyed in air, which produces much lower magnetizations during cooling.

In samples from the interval between 3.85 and 6.05 m pyrite was identified by its oxidation to magnetite, maghemite and finally to hematite, which causes an increase and subsequent decrease in magnetization (Fig. 8). The sulfide phase always oxidizes above 450 °C, suggesting that mostly euhedral pyrite is present (Passier et al., 2001). Thermomagnetic analyses of sediments from the sulfidic zone do not reveal any definite evidence of magnetic iron sulfide compounds like pyrrhotite or greigite.

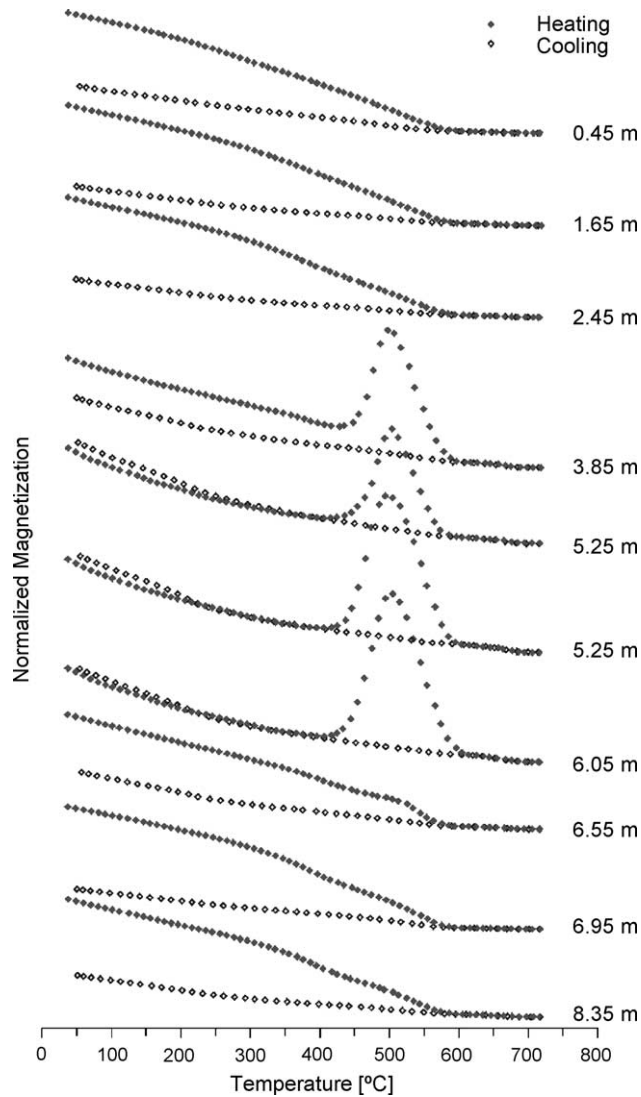


Fig. 8. Thermomagnetic cycles measured on a translation type Curie balance in air. Numbers on the right denote sample depths.

4.3. Scanning electron microscopy

Figs. 9 and 10 include representative micrographs of magnetic extracts together with X-ray spectra from microanalyses at selected spots. The elemental spectra could not be quantitatively evaluated, but provide valuable information to differentiate iron sulfide phases as well as to assess variations in the titanium content of iron oxides. Throughout the sediment column (titano-) magnetite is present, both as individual crys-

tals (Figs. 9a and b) and as intergrowths within silicates (Fig. 9c). Iron sulfides were only detected in the sulfidic zone (Fig. 10a–c), but nowhere above and below. Separate aggregates of sulfide minerals with uniform morphology and grain-size (Fig. 10b) strikingly resemble euhedral pyrite formed in laboratory experiments (Wang and Morse, 1996), which is consistent with conclusions from the thermomagnetic measurements.

Individual (titano-) magnetites are relatively large (commonly > 20 μm). Evidence for their low tempera-

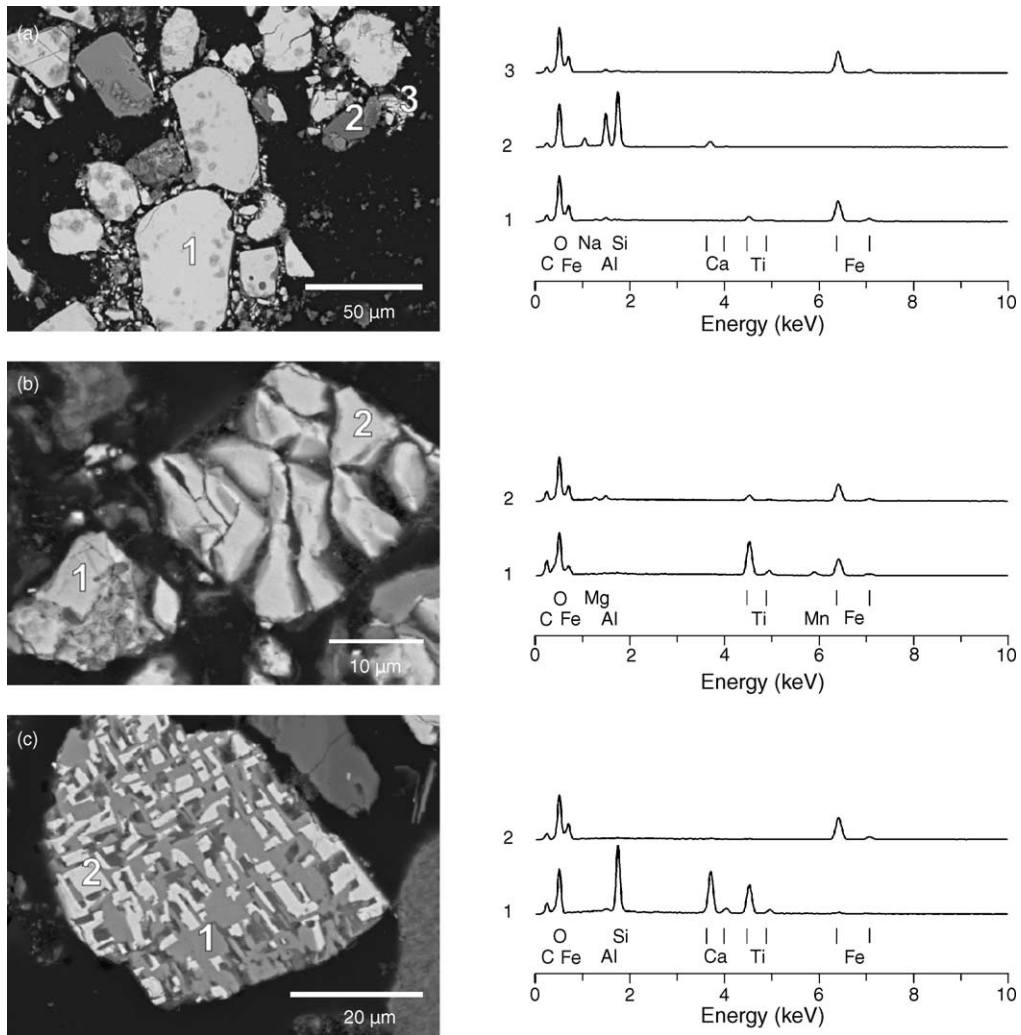


Fig. 9. Micrographs of magnetic extracts. (a) Cluster of small and large magnetic oxides (light gray) from the upper sediment series (2.45 m depth) containing titanomagnetite (1) and magnetite (3) with indications of limited maghemitization. Silicate minerals (2) appear dark gray. (b) Cluster of magnetic oxides from the lower sediment series (8.35 m depth) comprising titanomagnetite (1 and 2) with variable Ti content and advanced degree of maghemitization. (c) Intergrowth of a silicate (1) with magnetite (2) from the sulfidic zone (5.85 m depth). Element spectra are normalized to the oxygen peak.

ture oxidation is ubiquitous; in places, shrinkage cracks fragment the grains. High temperature dissolution patterns are more abundant in the lower sediment layers.

Although large individual crystals are still present in the sulfidic zone, (titano-) magnetite is mainly preserved as inclusions in silicate minerals, where the original magmatic structure was not disintegrated by erosion. Nevertheless, in part they are replaced by iron

sulfides (Fig. 10a). Apparently, this process mainly involves the larger crystals, whereas the smaller, well sheltered (titano-) magnetite fraction seems unaffected by alteration, which suggests that they might significantly contribute to the magnetic characteristics of the sulfidic zone. High temperature oxidized individual grains reveal extensive to complete dissolution of the low Ti titanomagnetite fraction, leaving the high

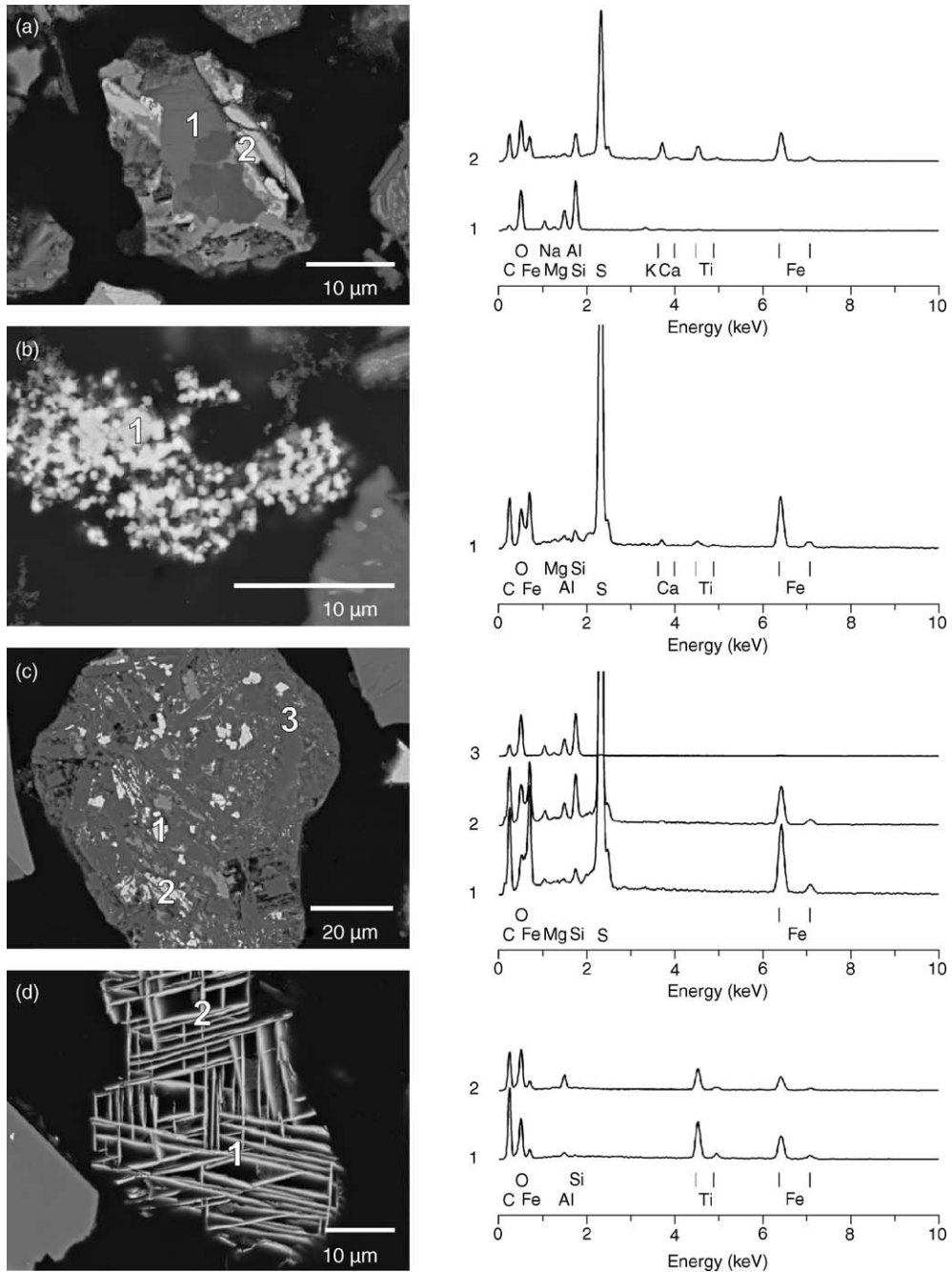


Fig. 10. Micrographs of magnetic extract from the sulfidic zone. (a, 5.25 m depth) Dark gray silicates (1) with iron sulfide overgrowth, identified as pyrite, probably replacing iron oxides. (b, 6.05 m depth) Cluster of euhedral pyrite (1) identified after Wang and Morse (1996). (c, 5.25 m depth) Iron sulfide minerals (white; 1 and 2) apparently replacing (titano)magnetite in a silicate matrix (3) which also contains fine grained iron oxide inclusions (light gray). (d, 6.55 m depth) High Ti titanohematite lamellae (1 and 2) resulting from high temperature oxidation. Note that the originally present magnetite intergrowth has been entirely dissolved. Element spectra are normalized to the oxygen peak.

Ti titanohematite lamellae fully intact (Fig. 10d). Such minerals were quite frequently found in the magnetic extracts from the sulfidic zone.

5. Discussion and conclusions

Enhanced influx of organic material and methane rising from deep sources are the two key factors that create a distinct geochemical scenario in the upper sedimentary column on the Argentine continental slope in front of the Rio de la Plata estuary. The present geochemical zonation has been established as a result of a drastic decrease in sedimentation rate from about 100 to 5 cm/kyr toward the end of the last glacial period (Riedinger et al., *in press*). It caused a rapid ascent of the SMT from greater depth to around its current position just a few meters below the sediment surface. At around the SMT, free sulfide in the pore water is generated by AOM.

The intensely reducing environment in the sulfidic zone, extending from depths of 3.9 to 6.6 m in the investigated sequence, has a strong impact on the magnetic mineral inventory. However, significant magnetic mineral modification already occurs in the upper 0.5 m of the sedimentary sequence, as documented by a marked decrease in M_{AR} (Fig. 3d). The position of the first magnetically important diagenetic horizon may also be related to the last glacial/interglacial transition (Riedinger et al., *in press*). Approximately 60% of the primary fine grained (titano-) magnetite fraction is dissolved at this level. A simultaneous lesser drop in isothermal remanent magnetization (Fig. 3e) indicates that about three quarters of the bulk ferrimagnetic mineral content persists in the sediments below where M_{AR}/M_{IR} and κ_{AR}/κ (Fig. 7c and d) delimit a substantial shift to coarser grain-sizes. None of the magnetic parameters hint at formation of bacterial magnetite, which is found elsewhere just above the iron-redox boundary (e.g., Karlin et al., 1987; Tarduno and Wilkison, 1996). As specified by M_{HIR} (Fig. 4a), higher coercivity iron oxides and hydroxides appear to be scarcely affected by alteration at this diagenetic front.

This mode of reductive diagenesis, driven by microbially mediated degradation of organic matter under suboxic conditions, has previously been reported for various marine settings. In continental margin regions, especially where upwelling gives rise to elevated con-

centrations of organic carbon in the sediments, quite severe diagenetic alterations are typically observed. A main reason for the relatively limited dissolution of the magnetic iron oxides in the study area is their uncommonly coarse grain-size spectrum (Fig. 9a–c). This agrees with the nature of coarse sedimentary deposits that reflect the offshore distribution of the Rio de la Plata fluvial load (Frenz et al., 2004).

The primary detrital magnetic mineralogy is dominated by (titano-) magnetite, which is most probably derived from the Paraná volcanic province and delivered by the Uruguay and Paraná rivers. Hematite and goethite contents, which are estimated to make up around one third of the total magnetic mineral assemblage, are remarkably depleted compared to most other regions of the South Atlantic (Pye, 1987; Balsam and Otto-Bliesner, 1995; Schmidt et al., 1999).

The sulfidic environment at around the SMT caused dissolution of more than 80% of the primary ferrimagnetic mineral fraction (Fig. 3). Even though large amounts of high coercivity compounds have also been lost, their relative concentration increases to approximately 50% of the total magnetic mineral content in the sulfidic zone. The comparatively higher resistance of hematite and goethite against diagenetic dissolution implies a lower reactivity towards sulfide than for (titano-) magnetite (Yamazaki et al., 2003; Liu et al., 2004; Emiroglu et al., 2004). According to literature data (Canfield et al., 1992; Haese et al., 2000), the opposite should be expected. The shift in magnetic mineralogy specifically results in considerably higher magnetic stabilities documented in a two- to three-fold increase in coercivities (Fig. 5). Further details of this phenomenon were quantified by an IRM component analysis (Fig. 6). A three component solution yields relative contributions to remanent magnetization of approximately 11.7, 75.6 and 12.7% for ‘soft’ (titano-) magnetite, ‘hard’ (titano-) magnetite/hematite and ‘hardest’ hematite/goethite fractions in the sulfidic zone compared to 57.9, 39.8 and 2.3% in the overlying suboxic sediments. The tentative identification of these mineral components is mainly based on their respective average half IRM acquisition fields $B_{1/2} M_{IRA}$ (Table 1). $B_{1/2} M_{IRA}$ of 39.0 and 42.2 mT of ‘soft’ (titano-) magnetite in the suboxic and sulfidic sediments are best compatible with pure magnetite or low Ti content titanomagnetite (Day et al., 1977). In the sulfidic zone, where their concentrations dramatically

decline, they should mainly persist as relatively fine grained inclusions in a silicate matrix (Fig. 9c). The second component has been labelled ‘hard’ (titano-) magnetite/hematite, because of strikingly higher $B_{1/2}$ M_{IRA} values of 81.9 mT in the suboxic and 90.5 mT in the sulfidic layers, which are most plausibly explained by titanomagnetite with a significant Ti content and/or an advanced degree of maghemitization (Fig. 9b). Hematite of appropriate grain-size is another suitable candidate (Kletetschka and Wasilewski, 2002) and possibly also Ti-rich titanohematite (Fig. 10d). For the third high coercivity component, which is characterized by $B_{1/2}$ M_{IRA} of 1000 and 887 mT in the suboxic and sulfidic sediments, goethite should primarily be responsible, probably with contributions from hematite.

Combined dissolution of iron oxides and enhanced solid phase sulfur concentrations suggest formation of authigenic iron sulfides at around the SMT. Thermomagnetic analyses only positively identified euhedral pyrite by its oxidation temperature above 450 °C in air (Fig. 8; Passier et al., 2001). On the other hand, high coercivities (Fig. 5) and an increasing $\sigma_{\text{rs}}/\sigma_{\text{s}}$ ratio (Fig. 7a) could hint at the presence of the ferrimagnetic iron sulfide mineral greigite (Fe_3S_4 ; Roberts, 1995), which has been repeatedly found in marine sediments. The reductive diagenetic sequence of iron oxide dissolution, metastable iron monosulfide and lastly stable pyrite formation is in principle well understood (Canfield and Berner, 1987). The intermediate phase greigite is ferrimagnetic and carries a stable intense magnetic remanence at room temperature (Berner, 1967; Goldhaber and Kaplan, 1974; Roberts and Turner, 1993; Wang and Morse, 1996; Wilkin and Barnes, 1996). Greigite might be preserved by arresting pyritization reactions, for example when pyrite forms as overgrowths on precursor minerals (Wang and Morse, 1996) or dissolved iron is produced at a faster rate than HS^- (Kao et al., 2004).

Scanning electron microscope observations indicate two types of iron sulfide: (1) pyrite replacing iron oxides as overgrowths on silicates (Fig. 10a) or as inclusions in a silicate matrix (Fig. 10c), and (2) agglomerates of pyrite crystals which display uniform shape and size (Fig. 10b). Wilkin and Barnes (1997) and Canfield and Berner (1987) concluded that the latter feature is the result of a single framboidal greigite nucleation event in pore waters containing low concentration of iron and sulfide. Iron limitation subsequently

leads to the formation of pyrite. The absence of dithionite soluble mineral phases, mainly iron oxides, hint at iron-limited pyritization processes (Raiswell and Canfield, 1996). Sequential extraction indeed confirmed low concentration of reactive iron phases in the sulfidic zone of Argentine continental slope sediments (Riedinger et al., in press).

Another interesting issue in the context of iron limitation is maghemitization, which proceeds through preferential diffusion of Fe^{2+} out of (titano-) magnetite as Fe^{2+} is more easily detached from the mineral structure than Fe^{3+} (Cornell and Schwertmann, 1996). SEM analyses provided widespread evidence for an advanced maghemitization indicated by surficial cracking within and below (Fig. 9b) the sulfidic zone, whereas in the upper sediment series only minor evidence of low temperature oxidation was found. These findings suggest that progressing maghemitization could be an important process in sulfidic environments. It will modify the magnetic characteristics of the residual (titano-) magnetite fraction by, as was observed, a decrease in grain-size and increased coercivities. Moreover, the preferential diffusion of Fe^{2+} out of (titano-) magnetite may give a hint to explaining the superior stability of hematite and titanohematite (Fig. 10d) under sulfidic conditions.

In the sulfidic sediments, grain-size variations (Fig. 7) indicate the opposite trend to that expected for iron oxide dissolution. The already coarse grained primary ferrimagnetic mineral assemblage loses almost all of its finer grained fraction at the first magnetically important diagenetic front under suboxic conditions. The subsequent strong diagenetic dissolution that affects all magnetic iron oxide minerals in the sulfidic environment will eventually cause a fining of the grain-size spectrum. Major factors contributing to this effect should be the small (titano-) magnetite grains preserved as inclusions in silicates and, possibly of prime importance, reduced effective magnetic grain-sizes, due to comprehensive fragmentation in the course of maghemitization (e.g., Cui et al., 1994).

The sediment series above and below the sulfidic zone reveal similar, though not identical magnetic characteristics which indicate that some alteration has also affected the lower part of the core during rapid passage of the SMT and prolonged exposure to a methanic environment. Under these conditions precipitation of authigenic minerals, such as iron sulfides,

iron and manganese carbonates and phosphates is likely (Berner, 1981). Thermomagnetic analyses (Fig. 8) did not identify a magnetic sulfide phase, specifically not at around 7 m, where a peculiar maximum is observed in the concentration indicative parameters (Figs. 3 and 4c). Other possible iron and manganese bearing authigenic mineralizations may form in the non-sulphidic sediments below the SMT (Berner, 1981; Sagnotti et al., 2005), such as siderite, rhodochrosite and vivianite, which are paramagnetic at room temperature, and can be identified with low temperature magnetic analyses. More work is clearly needed to better understand the magnetic mineral alteration in the lower part of the sediment column.

Acknowledgements

The authors thank T. Frederichs, D. Heslop, C. Hilgenfeldt and S. Kasten for their technical assistance and helpful comments. Thermomagnetic measurements and SEM analyses were carried out at Utrecht University. The people there are gratefully acknowledged for their hospitality and efficient cooperation. Reviews by Andrew Roberts and an anonymous referee helped to substantially improve this manuscript. This study was supported by the Deutsche Forschungsgemeinschaft (DFG) and the Netherlands Organization of Scientific Research (NWO), as part of the European Graduate College 'Proxies in Earth History'.

References

- Balsam, W.L., Otto-Bliesner, B.L., 1995. Modern and last glacial maximum eolian sedimentation patterns in the Atlantic Ocean interpreted from sediment iron oxide content. *Paleoceanography* 2, 531–542.
- Banerjee, S.K., King, J., Marvin, J., 1981. A rapid method of magnetic granulometry with applications to environmental studies. *Geophys. Res. Lett.* 8, 333–336.
- Berner, R.A., 1967. Thermodynamic stability of sedimentary iron sulfides. *Am. J. Sci.* 265, 773–785.
- Berner, R.A., 1981. A new geochemical classification of sedimentary environments. *J. Sediment. Petrol.* 51, 359–365.
- Bleil, U., et al., 1994. Report and preliminary results of Meteor Cruise M29/2. *Berichte, Fachbereich Geowissenschaften, Universität Bremen*, 59, 153 pp.
- Bleil, U., et al., 2001. Report and preliminary results of Meteor Cruise M46/3. *Berichte, Fachbereich Geowissenschaften, Universität Bremen*, 172, 161 pp.
- Bloemendal, J., King, J.W., Hall, F.R., Doh, S.-J., 1992. Rock magnetism of Late Neogene to Pleistocene deep-sea sediments: relationship to sediment source, diagenetic processes and sediment lithology. *J. Geophys. Res.* 97, 4361–4375.
- Boetius, A., Ravenschlag, K., Schubert, C.J., Rickert, D., Widdel, F., Gieseke, A., Amann, R., Jørgensen, B.B., Witte, U., Pfannkuche, O., 2000. A marine microbial consortium apparently mediating anaerobic oxidation of methane. *Nature* 407, 623–626.
- Borowski, W.S., Paull, C.K., Ussler, W., 1996. Marine pore-water sulfate profiles indicate in situ methane flux from underlying gas hydrate. *J. Geol.* 24, 655–658.
- Canfield, D.E., Berner, R.A., 1987. Dissolution and pyritization of magnetite in anoxic marine sediments. *Geochim. Cosmochim. Acta* 51, 645–659.
- Canfield, D.E., Raiswell, R., Bottrell, S., 1992. The reactivity of sedimentary iron minerals toward sulfide. *Am. J. Sci.* 292, 659–683.
- Channell, J.E.T., Hawthorne, T., 1990. Progressive dissolution of titanomagnetites at ODP site 653 (Tyrrhenian Sea). *Earth Planet. Sci. Lett.* 96, 469–480.
- Channell, J.E.T., Stoner, J.S., 2002. Plio-Pleistocene magnetic polarity stratigraphies and diagenetic magnetite dissolution at ODP Leg 177 Sites (1089, 1091, 1093 and 1094). *Mar. Micropaleontol.* 45, 269–290.
- Cornell, R.M., Schwertmann, U., 1996. *The Iron Oxides — Structure, Properties Reactions Occurrences and Uses*. VCH, Weinheim, 573 pp.
- Cui, Y., Verosub, K.L., Roberts, A.P., 1994. The effect of low-temperature oxidation on large multi-domain magnetite. *Geophys. Res. Lett.* 21, 757–760.
- Day, R., Fuller, M., Schmidt, V.A., 1977. Hysteresis properties of titanomagnetites: grain-size and compositional dependence. *Phys. Earth Planet. Inter.* 13, 260–266.
- Dekkers, M.J., Langereis, C.G., Vriend, S.P., van Santvoort, P.J.M., de Lange, G.J., 1994. Fuzzy c-means cluster analysis of early diagenetic effects on natural remanent magnetization acquisition in a 1.1 Myr piston core from the Central Mediterranean. *Phys. Earth Planet. Inter.* 85, 155–171.
- Dunlop, D.J., 2002. Theory and application of the Day plot (M_{rs}/M_s versus H_{cr}/H_c) 1. Theoretical curves and tests using titanomagnetite data. *J. Geophys. Res.*, 107, doi:10.1029/2001JB000486.
- Emiroglu, S., Rey, D., Petersen, N., 2004. Magnetic properties of sediment in the Ría de Arousa (Spain): dissolution of iron oxides and formation of iron sulphides. *Phys. Chem. Earth* 29, 947–959.
- Ewing, M., Eitrem, S.L., Ewing, J.I., Le Pichon, X., 1971. Sediment transport and distribution in the Argentine Basin. 3. Nepheloid layer and processes of sedimentation. *Phys. Chem. Earth* 8, 49–77.
- Ewing, M., Ludwig, W.J., Ewing, J.I., 1964. Sediment distribution in the oceans: the Argentine Basin. *J. Geophys. Res.* 69, 2003–2032.
- Frederichs, T., Bleil, U., Däumler, K., von Dobeneck, T., Schmidt, A.M., 1999. The magnetic view on the marine paleoenvironment: parameters, techniques and potentials of rock magnetic studies as a key to paleoclimatic and paleoceanographic changes. In: Fischer, G., Wefer, G. (Eds.), *Use of Proxies in Paleoceanography: Examples from the South Atlantic*. Springer-Verlag, Berlin, pp. 575–599.

- Frenz, M., Höppner, R., Stuu, J.-B., Wagner, T., Henrich, R., 2004. Surface sediment bulk geochemistry and grain-size composition related to oceanic circulation along the South American continental margin in the Southwest Atlantic. In: Wefer, G., Mulitza, S., Ratmeyer, V. (Eds.), *The South Atlantic in the late Quaternary: Reconstruction of Material Budget and Current Systems*. Springer-Verlag, Berlin, pp. 347–373.
- Froelich, P.N., Klinkhammer, G.P., Bender, M.L., Luedtke, N.A., Heath, G.R., Cullen, D., Dauphin, P., Hammond, D., Hartman, B., Maynard, V., 1979. Early oxidation of organic matter in pelagic sediments of the eastern equatorial Atlantic: suboxic diagenesis. *Geochim. Cosmochim. Acta* 43, 1075–1090.
- Goldhaber, M.B., Kaplan, I.R., 1974. The sulfur cycle. In: Goldberg, E.D. (Ed.), *The Sea*, vol. 5. John Wiley and Sons, New York, pp. 569–655.
- Gornitz, V., Fung, I., 1994. Potential distribution of methane hydrates in the world's oceans. *Glob. Biogeochem. Cycles* 8, 335–347.
- Haese, R.R., 1997. Beschreibung und Quantifizierung frühdiagenetischer Reaktionen des Eisens in Sedimenten des Südatlantiks. *Berichte, Fachbereich Geowissenschaften, Universität Bremen*, 99, 118 pp.
- Haese, R.R., Schramm, J., Rutgers van der Loeff, M.M., Schulz, H.D., 2000. A comparative study of iron and manganese diagenesis in continental slope and deep sea basin sediments, off Uruguay (SW Atlantic). *Int. J. Earth Sci.* 88, 619–629.
- Haese, R.R., Wallmann, K., Dahmke, A., Kretzmann, U., Müller, P.J., Schulz, H.D., 1997. Iron species determination to investigate early diagenetic reactivity in marine sediments. *Geochim. Cosmochim. Acta* 61, 63–72.
- Heider, F., Zitzelsberger, A., Fabian, F., 1996. Magnetic susceptibility and remanent coercive force in grown magnetite crystals from 0.1 μm to 6 mm. *Phys. Earth Planet. Inter.* 93, 239–256.
- Hensen, C., Zabel, M., Pfeifer, K., Schwenk, T., Kasten, S., Riedinger, N., Schulz, H.D., Boetius, A., 2003. Control of sulfate pore-water profiles by sedimentary events and the significance of anaerobic oxidation of methane for the burial of sulfur in marine sediments. *Geochim. Cosmochim. Acta* 67, 2631–2647.
- Heslop, D., Dekkers, M.J., Kruiver, P.P., van Oorschot, I.H.M., 2002. Automated fitting of isothermal remanent magnetisation acquisition curves using an expectation-maximisation algorithm. *Geophys. J. Int.* 148, 58–64.
- Kao, S.-J., Horng, C.-S., Roberts, A.P., Liu, K.K., 2004. Carbon–sulphur–iron relationships in sedimentary rocks from southwestern Taiwan: influence of geochemical environment on greigite and pyrrhotite formation. *Chem. Geol.* 203, 153–168.
- Karlin, R., 1990a. Magnetite diagenesis in marine sediments from the Oregon continental margin. *J. Geophys. Res.* 95, 4405–4419.
- Karlin, R., 1990b. Magnetic mineral diagenesis in suboxic sediments at Bettis site W-N, NE Pacific Ocean. *J. Geophys. Res.* 95, 4421–4436.
- Karlin, R., Levi, S., 1983. Diagenesis of magnetic minerals in recent haemipelagic sediments. *Nature* 303, 327–330.
- Karlin, R., Lyle, M., Heath, G.R., 1987. Authigenic magnetite formation in suboxic marine sediments. *Nature* 326, 490–493.
- Kasten, S., Freudenthal, T., Gingele, F.X., Schulz, H.D., 1998. Simultaneous formation of iron-rich layers at different redox boundaries in sediments of the Amazon deep-sea fan. *Geochim. Cosmochim. Acta* 62, 2253–2264.
- Kletetschka, G., Wasilewski, P.J., 2002. Grain size limit for SD hematite. *Phys. Earth Planet. Inter.* 129, 173–179.
- Kruiver, P.P., Dekkers, M.J., Heslop, D., 2001. Quantification of magnetic coercivity components by the analysis of acquisition curves of isothermal remanent magnetisation. *Earth Planet. Sci. Lett.* 189, 269–276.
- Larrasoana, J.C., Roberts, A.P., Stoner, J.S., Richter, C., Wehausen, R., 2003. A new proxy for bottom-water ventilation in the eastern Mediterranean based on diagenetically controlled magnetic properties of sapropel-bearing sediments. *Palaeogeogr. Palaeoclimatol. Palaeoecol.* 190, 221–242.
- Ledbetter, M.T., Klaus, A., 1987. Influence of bottom currents on sediment texture and sea-floor morphology in the Argentine Basin. In: Francis, T.J.G., Weaver, P.P.E. (Eds.), *Geology and Geochemistry of Abyssal Plains*. *Geol. Soc. London, Spec. Pub.*, 31, pp. 21–31.
- Liu, J., Zhu, R., Roberts, A.P., Li, S., Chang, J.-H., 2004. High-resolution analysis of early diagenetic effects on magnetic minerals in post-middle-Holocene continental shelf sediments from the Korea Strait. *J. Geophys. Res.* 109, doi:10.1029/2003JB002813.
- Lyle, M., 1983. The brown-green color transition in marine sediments: a marker of the Fe(III)–Fe(II) redox boundary. *Limnol. Oceanogr.* 28, 1026–1033.
- Maher, B.A., 1988. Magnetic properties of some synthetic submicron magnetites. *Geophys. J.* 94, 83–96.
- Manley, P.M., Flood, R.D., 1993. Paleoflow history determined from mudwave migration: Argentine Basin, Atlantic. *Geochim. Cosmochim. Acta* 60, 243–263.
- Memery, L., Arhan, M., Alvarez-Salgado, X.A., Messias, M.-J., Mercier, H., Castro, C.G., Rios, A.F., 2000. The water masses along the western boundary of the south and equatorial Atlantic. *Progr. Oceanogr.* 47, 69–98.
- Mullender, T.A.T., van Velzen, A.J., Dekkers, M.J., 1993. Continuous drift correction and separate identification of ferrimagnetic and paramagnetic contributions in thermomagnetic runs. *Geophys. J. Int.* 114, 663–672.
- Neretin, L.N., Böttcher, M.E., Jørgensen, B.B., Volkov, I.I., Lüschen, H., Hilgenfeldt, K., 2004. Pyritization processes and greigite formation in the advancing sulfidization front in the Upper Pleistocene sediments of the Black Sea. *Geochim. Cosmochim. Acta* 68, 2081–2093.
- Niewöhner, C., Hensen, C., Kasten, S., Zabel, M., Schulz, H.D., 1998. Deep sulphate reduction completely mediated by anaerobic methane oxidation in sediments of the upwelling area off Namibia. *Geochim. Cosmochim. Acta* 62, 455–464.
- Passier, H.F., de Lange, G.J., Dekkers, M.J., 2001. Magnetic properties and geochemistry of the active oxidation front and the youngest sapropel in the eastern Mediterranean Sea. *Geophys. J. Int.* 145, 604–614.
- Petersen, N., von Dobeneck, T., Vali, H., 1986. Fossil bacterial magnetite in deep-sea sediments from the South Atlantic Ocean. *Nature* 320, 611–615.
- Pye, K., 1987. *Aeolian Dust and Dust Deposits*. Academic Press, London, 334 pp.

- Raiswell, R., Canfield, D.E., 1996. Rates of reaction between silicate iron and dissolved sulfide in Peru Margin sediments. *Geochim. Cosmochim. Acta* 60, 2777–2787.
- Richardson, M.J., Weatherly, G.L., Gardner, W.D., 1993. Benthic storms in the Argentine Basin. *Deep-Sea Res. II* 40, 975–987.
- Reitz, A., Hensen, C., Kasten, S., Funk, J.A., de Lange, G.J., 2004. A combined geochemical and rock-magnetic investigation of a redox horizon at the last glacial/interglacial transition. *Phys. Chem. Earth* 29, 921–931.
- Riedinger, N., Pfeifer, K., Kasten, S., Garming, J.F.L., Vogt, C., Hensen, C., in press. Diagenetic alteration of magnetic signals by anaerobic oxidation of methane related to a change in sedimentation rate. *Geochim. Cosmochim. Acta*.
- Roberts, A.P., 1995. Magnetic properties of sedimentary greigite (Fe_3S_4). *Earth Planet. Sci. Lett.* 134, 227–236.
- Roberts, A.P., Turner, G.M., 1993. Diagenetic formation of ferrimagnetic iron sulphide minerals in rapidly deposited marine sediments, South Island, New Zealand. *Earth Planet. Sci. Lett.* 115, 257–273.
- Roberts, A.P., Stoner, J.S., Richter, C., 1999. Diagenetic magnetic enhancement of sapropels from the eastern Mediterranean Sea. *Mar. Geol.* 153, 103–116.
- Robertson, D.J., France, D.E., 1994. Discrimination of remanence-carrying minerals in mixtures, using isothermal remanent magnetization acquisition curves. *Phys. Earth Planet. Inter.* 82, 223–234.
- Robinson, S.G., Sahota, J.T.S., Oldfield, F., 2000. Early diagenesis in North Atlantic abyssal plain sediments characterized by rock-magnetic and geochemical indices. *Mar. Geol.* 163, 77–107.
- Sagnotti, L., Roberts, A.P., Weaver, R., Verosub, K.L., Florindo, F., Pike, C.R., Clayton, T., Wilson, G.S., 2005. Apparent magnetic polarity reversals due to remagnetization resulting from late diagenetic growth of greigite from siderite. *Geophys. J. Int.* 160, 89–100.
- Schmidt, A.M., von Dobeneck, T., Bleil, U., 1999. Magnetic characterization of Holocene sedimentation in the South Atlantic. *Paleoceanography* 14, 465–481.
- Schulz, H.D., Dahmke, A., Schinzel, U., Wallmann, K., Zabel, M., 1994. Early diagenetic processes, fluxes, and reaction rates in sediments of the South Atlantic. *Geochim. Cosmochim. Acta* 58, 2041–2060.
- Schulz, H.D., et al., 2001. Report and preliminary results of Meteor Cruise M46/2. *Berichte, Fachbereich Geowissenschaften, Universität Bremen*, 184, 107 pp.
- Stevenson, F.J., Cheng, C.-N., 1969. Amino acid levels in the Argentine Basin sediments: correlation with Quaternary climatic changes. *J. Sediment. Petrol.* 39, 345–349.
- Stoner, J.S., Channell, J.E.T., Hillaire-Marcel, C., 1996. The magnetic signature of rapidly deposited detrital layers from the deep Labrador Sea: relationship to North Atlantic Heinrich layers. *Paleoceanography* 11, 309–325.
- Tarduno, J.A., Wilkison, S.L., 1996. Non-steady state magnetic mineral reduction, chemical lock-in, and delayed remanence acquisition in pelagic sediments. *Earth Planet. Sci. Lett.* 144, 315–326.
- Thompson, R., Oldfield, F., 1986. *Environmental Magnetism*. Allen & Unwin, London, 227 pp.
- von Dobeneck, T., 1996. A systematic analysis of natural magnetic mineral assemblages based on modeling hysteresis loops with coercivity-related hyperbolic basis functions. *Geophys. J. Int.* 124, 675–694.
- Wang, Q., Morse, J.W., 1996. Pyrite formation under conditions approximating those in anoxic sediments I. Pathway and morphology. *Mar. Chem.* 52, 99–121.
- Wilkin, R.T., Barnes, H.L., 1996. Pyrite formation by reactions of iron monosulfides with dissolved inorganic and organic sulfur species. *Geochim. Cosmochim. Acta* 60, 4167–4179.
- Wilkin, R.T., Barnes, H.L., 1997. Formation processes of framboidal pyrite. *Geochim. Cosmochim. Acta* 61, 323–339.
- Yamazaki, T., Abdeldayem, A.L., Ikehara, K., 2003. Rock-magnetic changes with reduction diagenesis in Japan Sea sediments and preservation of geomagnetic secular variation in inclination during the last 30,000 years. *Earth Planets Space* 55, 327–340.